

Article

A Novel Immune-Related Gene Prognostic Index (IRGPI) in Pancreatic Adenocarcinoma (PAAD) and Its Implications in the Tumor Microenvironment

Shujing Zhou ^{1,2}, Szöllösi Attila Gábor ³, Xufeng Huang ^{1,4}, Yi Che Chang Chien ^{5,*}, and András Hajdu ^{1*}¹ Department Data Science and Visualization, University of Debrecen, Debrecen 4028, Hungary.² Faculty of Medicine, University of Debrecen, Debrecen 4032, Hungary.³ Department of Immunology, University of Debrecen, Debrecen 4032, Hungary.⁴ Faculty of Dentistry, University of Debrecen, Debrecen 4032, Hungary.⁵ Department of Pathology, University of Debrecen, Debrecen 4032, Hungary.* Correspondence: Yi Che Chang Chien and András Hajdu (hajdu.andras@inf.unideb.hu)

Citation: Lastname, F.; Lastname, F.; Lastname, F. Title. *Cancers* **2022**, *14*, x. <https://doi.org/10.3390/xxxxx>

Academic Editor: Firstname Lastname

Received: date
Accepted: date
Published: date

Publisher's Note: MDPI stays neutral with regard to jurisdictional claims in published maps and institutional affiliations.



Copyright: © 2022 by the authors. Submitted for possible open access publication under the terms and conditions of the Creative Commons Attribution (CC BY) license (<https://creativecommons.org/licenses/by/4.0/>).

Abstract: Purpose: Pancreatic adenocarcinoma (PAAD) is one of the most lethal malignancies, with less than 10% of patients surviving more than 5 years. Existing biomarkers for reliable survival rate prediction need to be enhanced. As a result, the objective of this study was to create a novel immune-related gene prognostic index (IRGPI) for estimating overall survival (OS) and to analyze the molecular subtypes based on this index. **Materials and procedures:** RNA sequencing and clinical data were retrieved from publicly available sources and analyzed using several R software packages. A unique IRGPI and optimum risk model were developed using a machine learning algorithm. The prediction capability of our model was then compared to that of previously proposed models. A correlation study was also done between the immunological tumor microenvironment, risk groups, and IRGPI genes. Furthermore, we classified PAAD into different molecular subtypes based on the expression of IRGPI genes and investigated their features in tumor immunology using the K-means clustering technique. **Results:** A 12-gene IRGPI (FYN, MET, LRSAM1, PSPN, ERAP2, S100A1, IL20RB, MAP3K14, SEMA6C, PRKCG, CXCL11, and GH1) was established and verified along with a risk model. OS prediction by our model outperformed previous gene signatures. According to the findings of our correlation studies, different risk groups and IRGPI genes were found to be tightly related to tumor microenvironments, and PAAD could be further subdivided into immunologically distinct molecular subtypes based on the expression of IRGPI genes. **Conclusion:** The current study constructed and verified a unique IRGPI. Furthermore, our findings revealed a connection between the IRGPI and the immunological microenvironment of tumors. PAAD was differentiated into several molecular subtypes that might react differently to immunotherapy. These findings could provide new insights for precision and translational medicine for more innovative immunotherapy strategies.

Keywords: pancreatic cancer; machine learning; gene signature; molecular subtypes; tumor microenvironment

Introduction

Despite the rapid development of modern therapeutic interventions in cancer progression, improvement in pancreatic adenocarcinoma (PAAD) survival is still limited, with less than 10% of patients surviving 5 years after the discovery of the tumor ^{[1],[2]}. Currently, surgery and chemotherapy remain the mainstream in PAAD treatment ^{[3]-[7]}. Since such interventions result in high morbidity and mortality, enrichment of the arsenal of translational medicine is urgently needed ^{[8],[9]}.

The situation, however, is not encouraging. Although in clinical observations and animal modeling a handful of validated biomarkers such as KRAS, TP53, SMAD4, and CDKN2A, were found to exert positive effects on tumorigenesis, metastasis, and concomitantly poor prognosis, they were still believed to be insufficient to cause the disease and cannot be effectively utilized in targeting drug discovery ^{[10]-[16]}.

Due to the development of bioinformatic analytics, gene signatures identified from diverse representative gene sets of well-defined tumor stages are increasingly accepted as novel tumor marker candidates. In the most recent decade, various newly defined cell death mechanisms like ferroptosis and pyroptosis are expected to offer new insights into cancer development and cures ^{[17]-[19]}. Therefore, gene signatures derived from these two groups for prognostic prediction are “hot” research topics. On the other hand, tumor immunology, serving as the basis for immunotherapy which is proven to be successful in certain cancer types, was investigated to a much more limited degree in gene signature development, particularly in PAAD ^{[20],[21]}. Therefore, the present study established a novel immune-related gene prognostic index (IRGPI) for overall survival (OS) estimation for PAAD patients, and explored more precise molecular subtypes in PAAD, together with corresponding immune characteristics.

The following demonstrates the workflow of the present study (Fig 1).

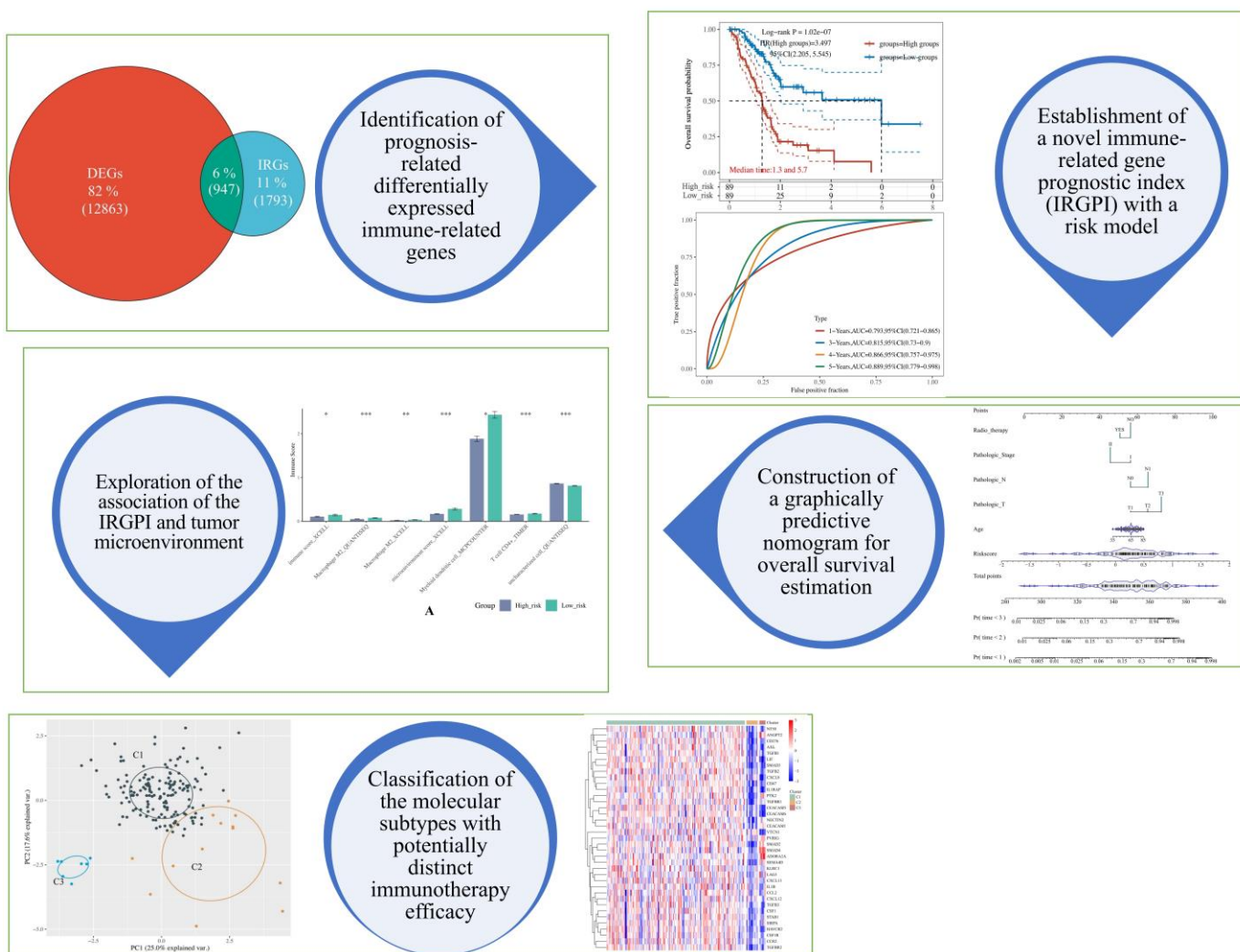


Figure 1. The Graphical abstract of the present study. In this work, we first screened the prognosis-related differentially expressed immune-related genes in pancreatic adenocarcinoma (PAAD) to select feature genes (i.e., the 12 genes within the immune-related gene prognostic index) to construct a machine learning model. Then, we compared its predictive performance with previous models derived from ferroptosis and pyroptosis, finding that our model performed better. Next, we integrated other clinical factors such as age, pathological stage, as well as others to build a nomogram so that clinicians could use it graphically. Afterward, we explored the potential relationship between our model and the tumor microenvironment. Finally, we used unsupervised clustering to classify PAAD patients into 3 more precise molecular subtypes according to the expression of the IRGPI genes.

Materials and methods

Data acquisition and processing

The RNA-seq data and corresponding clinical information of TNBC patients were downloaded from The Cancer Genome Atlas (TCGA) cohort (<https://www.genome.gov/Funded-Programs-Projects/Cancer-Genome-Atlas>), International Cancer Genome Consortium (ICGC) data portal (<https://dcc.icgc.org/>), and Gene Expression Omnibus (GEO) database

(<https://www.ncbi.nlm.nih.gov/geo/>). The well-organized data was divided into a TCGA training set (N=177), an ICGC validation set (from Australian patients, N=269), and a GEO validation set (from the GSE62452 dataset, N=130) [22],[23]. Additionally, 54 non-tumorous samples from the Genotype-Tissue Expression (GTEx) project (<https://gtexportal.org>) and unique immune-related genes (IRGs) from the ImmPort database (<https://www.immport.org>) were also integrated into the analytics [24],[25]. The R software packages involved in the present study were embedded in R Foundation (v 4.0.3) and the GSCA platform (<http://bioinfo.life.hust.edu.cn/GSCA/>) [26]. Except for special notification, statistical tests were done based on the Spearman method, and P-value < 0.05 and/or FDR < 0.05 was deemed statistically significant in the present study.

Identification of prognosis-related differentially expressed immune-related genes (DEIRGs)

The R package “limma” was used to identify differentially expressed genes (DEGs) [27]. The volcano plot was plotted by R package “ggplot2” to visualize the DEGs [28]. Furthermore, the Venn diagram was drawn by JVenn to demonstrate the number and percentage of differentially expressed immune-related genes (DEIRGs) [29]. Log-rank tests and univariate Cox proportional hazard regression were conducted to screen the prognosis-related DEIRGs.

Establishment of immune-related gene prognostic index (IRGPI) and risk model

The Least Absolute Shrinkage and Selection Operator (LASSO) penalized Cox proportional hazards regression was applied to train the optimal risk model by the R package “glmnet” [30]. The calculation of the risk score was completed after the removal of overfitting. The risk score was calculated by the following formula:

$$\text{Risk score} = \sum_{i=1}^n (\text{Exp}_i * \text{coef}_i),$$

where n is the number of prognostic genes, Exp_n is the expression level of a specific gene, and coef_n is the regression coefficient of a specific gene in the multi-Cox regression. The patients were further divided into high- and low-risk groups according to the median value of the risk score. The Kaplan Meier (KM) survival curves for OS analysis were also plotted as well as the time-dependent receiver operating characteristic (ROC) curve (for 1-, 3-, and 5-year survival) through R packages “survival” and “timeROC” [31],[32].

Comparison with previously proposed predictors

We compared the predictive performance of previous risk models derived from ferroptosis and pyroptosis in the TCGA training and ICGC validation sets. Of note that due to the lack of statistical significance between the high- and low-risk groups classified by both models in the GSE62452 dataset, such analytics could not be conducted. As a complement, we also employed the decision curve analysis (DCA) that was done by R package “rmda” to compare the clinical value of each model.

Construction of predictive nomogram according to the risk model

Combined with multiple clinical factors (i.e., age, genders, TNM stages, pathological stages, histological grades, radiotherapy), a univariate and multivariate Cox regression was performed. Besides, according to the risk model, we further constructed a nomogram that contains only prognosis-related factors, through which the OS rate in given years could be estimated graphically.

Assessment of the immunological tumor microenvironment

The general appearance of the tumor microenvironment was assessed by the R package “ESTIMATE”^[36], while for the analysis of the abundance of various immune cell types, we curated relevant data from Tumor IMMune Estimation Resource 2.0 (TIMER 2.0) (<http://timer.cistrome.org/>) portal and processed it by the R package “immunedeconv” through 6 algorithms (i.e., TIMER, XCELL, MCPCOUNTER, CIBERSORT, EPIC, and QUANTISED)^{[33]-[36]}.

Unsupervised Consensus Clustering

According to the IRGPI, the samples of the TCGA training set were divided into subgroups utilizing consensus clustering with the R package “ConsensusClusterPlus”^[37]. Then, we checked the expression of IRGPI genes in each molecular subtype to further confirm their eligibility as classifying standards. Each subtype was followed by survival analysis.

Results

12 feature genes were selected to construct the prognosis predictor through the LASSO algorithm

177 PAAD samples from the TCGA cohort and 54 normal samples from the GTEx project were acquired for analysis giving rise to 12,863 DEGs (Fig 2 A). 947 DEIRGs were extracted via intersecting with the immune-related gene list provided by the ImmPort database (Fig 2 B). Eventually, survival analysis revealed that 149 genes were significantly related to the OS of PAAD patients (Supplementary S1).

Then, we employed the LASSO algorithm to select the feature genes to construct the prognosis predictor with the L1 norm penalized, through which 12 genes (i.e., FYN, MET, LRSAM1, PSPN, ERAP2, S100A1, IL20RB, MAP3K14, SEMA6C, PRKCG, CXCL11, and GH1) were filtered as at this point the corresponding lambda value was minimized to 0.0986 (Supplementary S2).

Afterward, an over-representation analysis was conducted. The results indicated that the most enriched gene ontology (GO) term was “regulation of response to stimulus”, followed by “response to external stimulus” (Fig 2 C), and the most enriched Kyoto encyclopedia of genes and genomes (KEGG) pathway was “Axon guidance”, followed by “Focal adhesion”, “Cytokine-cytokine receptor interaction”, and “MAPK signaling pathway” (Fig 2 D).

In addition, the expression of each IRGPI gene in both normal and tumorous samples was compared. As a result, except for GH1, they were found relatively higher expressed in tumorous samples (Supplementary S3).

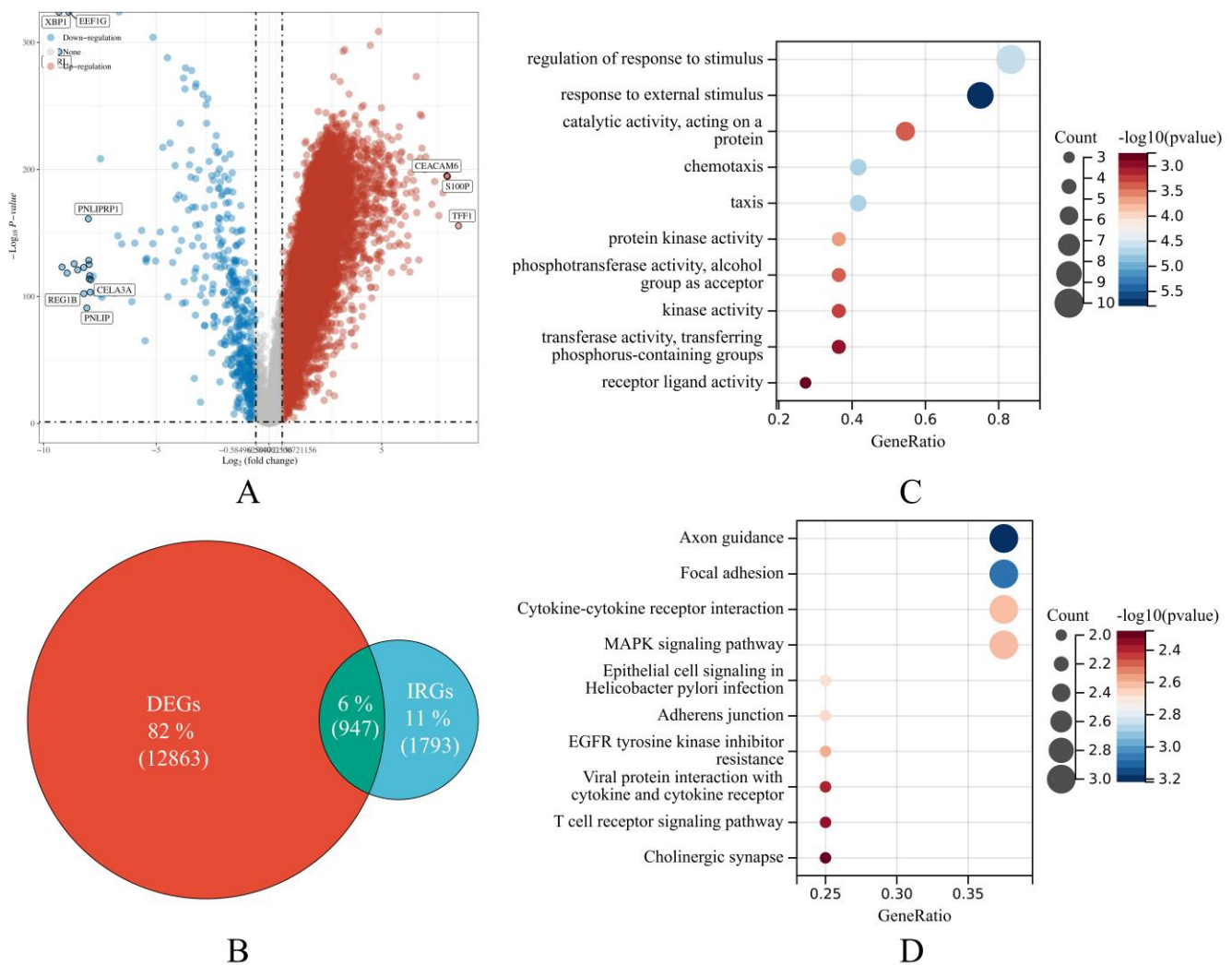


Figure 2. Feature gene selection and overrepresentation analysis outcomes. (A) The volcano plot displays the differentially expressed genes (DEGs) in pancreatic adenocarcinoma (PAAD) according to the TCGA data. The spots represent genes. The top 10 DEGs were labeled. Red shows up-regulated expression in tumorous tissues than normal samples, whereas blue represents the reverse. Non-DEGs are in gray. (B) The Venn diagram demonstrates the intersection of interest. The green region of the Venn diagram shows the number and ratio of DEIRGs. The red and blue sections show DEGs and immune-related genes (IRGs), respectively. (C)-(D) The bubble plots show gene ontology (GO) and Kyoto encyclopedia of genes and genomes (KEGG) pathway over-representation analyses. The size of the bubble corresponds to the number of genes from our samples found in the GO or KEGG pathway. P-value < 0.05 and FDR < 0.05 are statistically significant.

IRGPI-based risk model demonstrated a strong predictive power

After minimizing the overfitting and reaching the minimal lambda value, a mathematical formula for risk score calculation was set as follows:

$$\text{Risk score} = (-0.0334) * \text{FYN} + (0.2101) * \text{MET} + (-0.0956) * \text{LRSAM1} + (-0.2048) * \text{PSPN} + (0.0343) * \text{ERAP2} + (-0.0159) * \text{S100A1} + (0.0664) * \text{IL20RB} + (-0.0907) * \text{MAP3K14} + (-0.0437) * \text{SEMA6C} + (-0.0198) * \text{PRKCG} + (0.0716) * \text{CXCL11} + (-0.3634) * \text{GH1}$$

The above formula was then applied to the ICGC and GEO validation sets. We divided the samples into high- and low-risk groups using the risk score's

median value. It turned out that the OS probability was significantly worse in high-risk patients than that in low-risk patients in all datasets. The median survival time for the high-risk group in the TCGA training set is 1.3 years, while that of the low-risk group is 5.7 years (Fig 3 A). The median survival time for the high-risk group in the ICGC validation set is 1.2 years, while that of the low-risk group is 1.7 years (Fig 3 B). The median survival time for the high-risk group in the GEO validation set is 12.6 months, while that of the low-risk group is 23.6 months (Fig 3 C).

The AUC values in TCGA training set were 0.793, 0.815, 0.866, 0.889 in 1-, 3-, 4-, and 5-year OS (Fig 3 D), and those in the ICGC validation set were 0.674, 0.525, 0.643, 0.835 (Fig 3 E). The AUC values in the GEO validation set were 0.543, 0.762, 0.82, and 0.891 in 1-, 2-, 3-, and 5-year OS (Fig 3 F). In general, an AUC value over 0.7 is considered a good model, and given the fact that the different database has different criteria for patient selection, the potential deviation during the validation was reasonable [38],[39]. Comprehensively speaking, the result should be deemed acceptable.

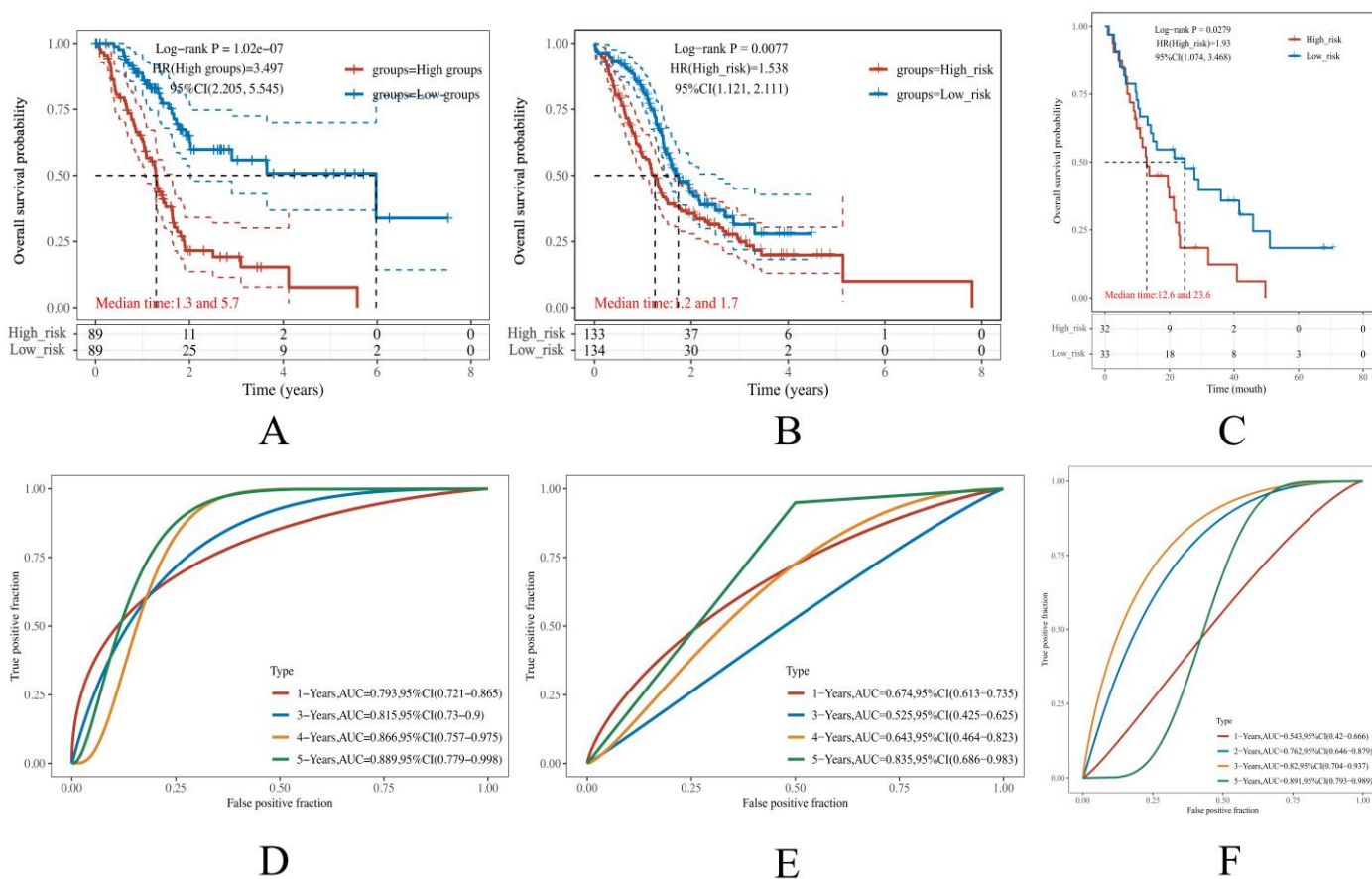


Figure 3. Construction of the immune-related gene prognostic index (IRGPI)-based risk model. (A)-(C) The Kaplan Meier (KM) curves demonstrate the overall survival (OS) rate of PAAD patients in the TCGA, ICGC, and GEO datasets, respectively. (D)-(F) The time-dependent receiver operating characteristics (ROC) curves of our risk model performed in the TCGA, ICGC, and GEO datasets, respectively. The larger the area under the curve (AUC), the more reliable the model.

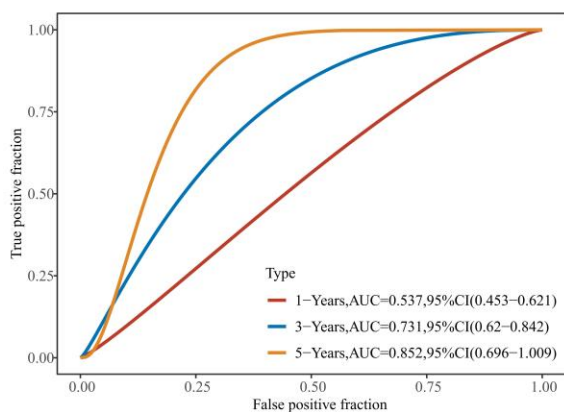
The predictive performance of the IRGPI-based risk model is superior to that of the ferroptosis- and pyroptosis-derived model

Gene signatures derived from ferroptosis and pyroptosis are hot research topics recently. However, whether the corresponding risk models are better than ours remains unknown. For this purpose, previously proposed ferroptosis- and pyroptosis-derived risk models were tested in the TCGA, ICGC, and GEO datasets to compare with our model.

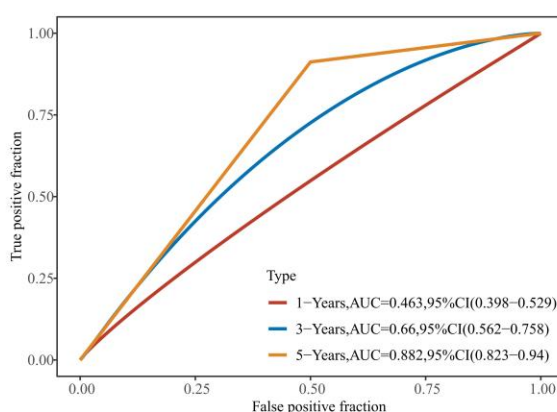
As a result, in the TCGA training set, the AUC values of Yang's ferroptosis model were 0.537, 0.731, and 0.852 for 1-, 3-, and 5-year OS (Fig 4 A). The AUC values of Bai's pyroptosis model were 0.737, 0.757, and 0.79 for 1-, 3-, and 5-year OS (Fig 4 C). In the ICGC dataset, the AUC values of Yang's ferroptosis model were 0.463, 0.66, and 0.882 for 1-, 3-, and 5-year OS (Fig 4 B), and those of Bai's pyroptosis model were 0.7, 0.525, 0.784 for 1-, 3-, and 5-year OS (Fig 4 D). Notably, due to the lack of statistical significance between the high- and low-risk groups classified by both models in the GSE62452 dataset, such analytics could not be conducted, while our model still worked robustly (Fig 3 F).

We additionally evaluated the predictive performance through the DCA diagram. Through the diagrams, it was observed that in the TCGA training set, the curve of our model was located superior to the others, suggesting that the corresponding performance was better (Fig 4 E). In the ICGC dataset, our model functioned slightly better than the other models in 3- and 5-year OS predictions but was less convincing than Bai's model in the 1-year OS prediction. (Fig 4 F).

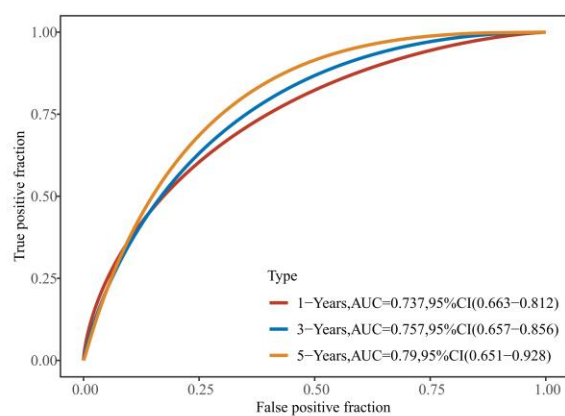
Overall, the predictive performance of our model was considered superior to that of Yang's and Bai's models.



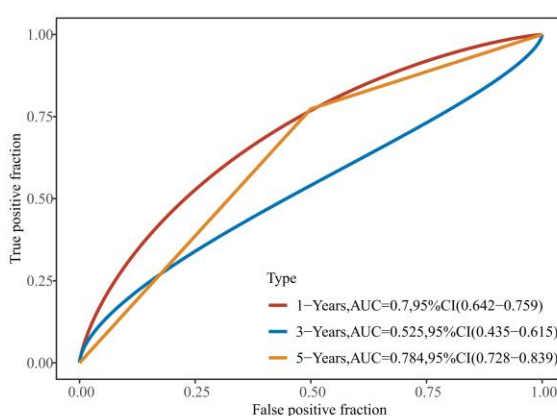
A



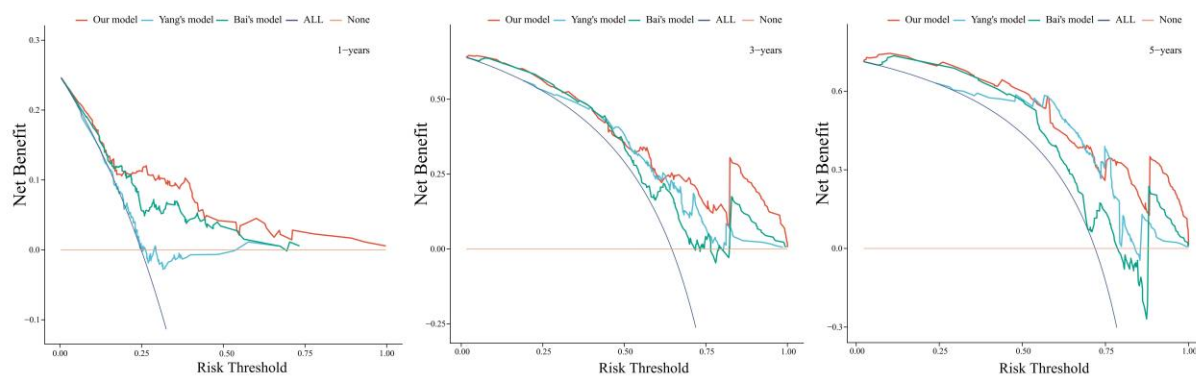
B



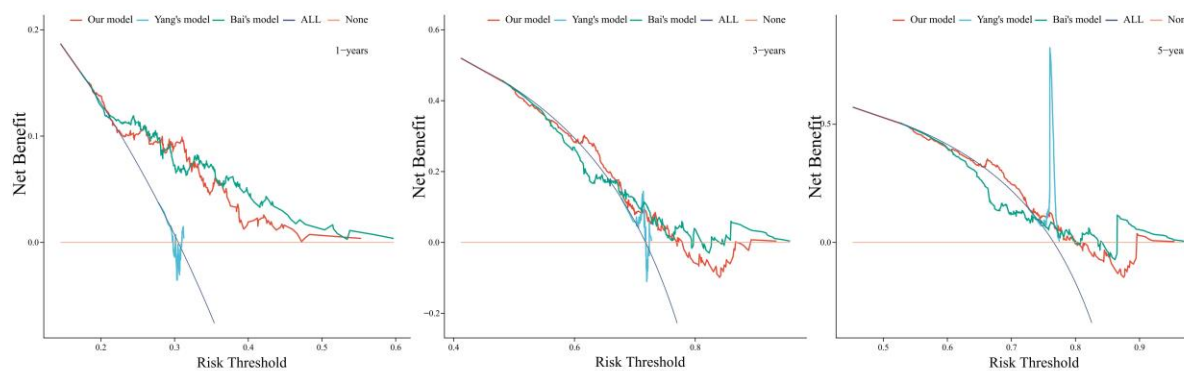
C



D



E



F

Figure 4. Comparison of the predictive performance of different models. (A)-(B) The time-dependent receiver operative characteristics (ROC) curve of Yang's ferroptosis-derived model in the TCGA and ICGC datasets, respectively. (C)-(D) The time-dependent ROC curve of Bai's pyroptosis-derived model in the TCGA and ICGC datasets, respectively. The larger the area under the curve (AUC), the more reliable the model. (E)-(F) The decision curve analysis (DCA) diagrams demonstrate the comparison of our risk model, Yang's ferroptosis-derived model, and Bai's pyroptosis-derived model in the TCGA and ICGC datasets, respectively. All: all positive; None: all negative. These serve as extreme conditions to determine background references. The distance from these extremes indicates a better clinical benefit that the corresponding model can achieve.

The risk score can serve as an independent prognostic indicator

Prognosis is usually linked to diverse clinical factors such as age, gender, pathological stage, and histological grades, among others. Therefore, we conducted univariate Cox regression to examine if the risk score was prognosis-related, and multivariate Cox regression to see if it was an independent prognostic indicator, both along with clinical factors. Subsequently, it was found that the risk score, age, T stage, N stage, pathological stages, and radiotherapy were prognosis-related, but only the risk score could serve as an independent prognosis indicator (Fig 5 A-B).

Then, we constructed a nomogram that integrated the risk score and all the prognosis-related clinical factors, through which the prediction could be done by measuring the corresponding points given specific risk scores and other clinical factors were known. The C-index of the nomogram was 0.786 (Fig 5 C). As usual, a C-index over 0.7 is thought to be good at classifying various objects, our constructed nomogram should be deemed excellent. The corresponding calibration curves were also plotted to demonstrate the comparison between the observed and the predictive values. It was found that the 1-, 2-, and 3-year predictive results possessed a good agreement with the ideal line, suggesting that our nomogram predicts the OS rate accurately (Fig 5 D).

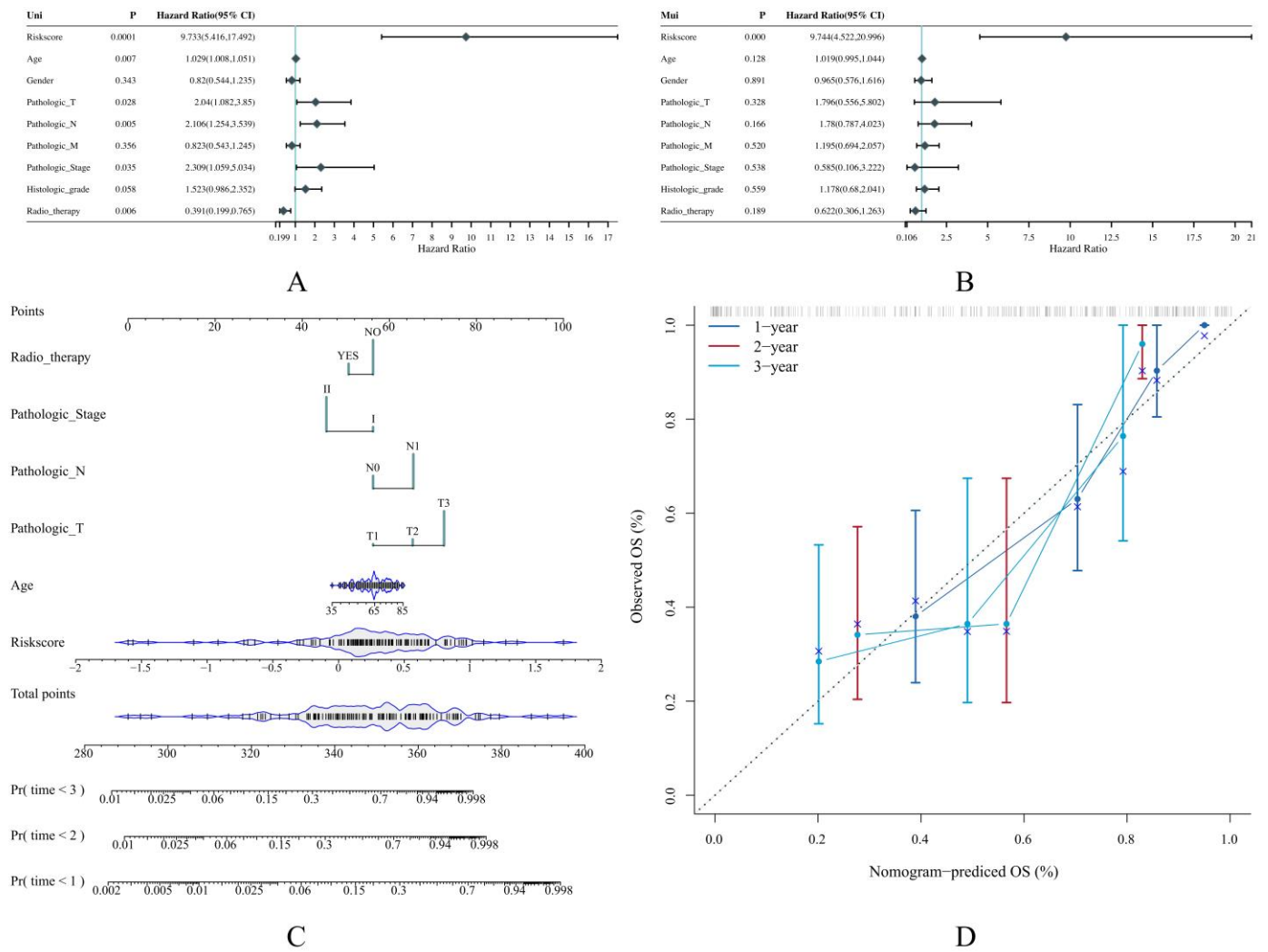


Figure 5. The establishment of a predictive nomogram according to our risk model. (A)-(B) The forest plot demonstrates the result of univariate and multivariate Cox regression for the risk score and other clinical factors such as age, gender, etc., respectively. (C)-(D) The nomogram and its calibration curve that contains prognosis-related factors identified from univariate Cox regression. The dashed line in the calibration curve is the ideal line representing 100% accuracy. The more closely the ideal line to the curve, the more precise prediction the corresponding model can make.

The risk score and IRGPI genes are tightly associated with the tumor microenvironment

Research in the recent decade has suggested that the tumor microenvironment plays an important role in the immunosuppressive phenomenon of pancreatic cancer through various mechanisms, both the well-understood ones such as the limited immune cell infiltration caused by mechanical constraints and the less-known ones in which the complicated crosstalks between the tumor cells, the desmoplastic stroma, and the immune cells significantly inhibits the normal anti-tumorous function of the T cells [40]-[42]. From this point of view, we elucidated the difference in 119 immune-related scores in high- and low-risk groups by integrating 7 immuno-informatical algorithms (i.e., TIMER, CIBERSORT, CIBERSORT-ABS, QUANTISED, MCPOUNTER, XCELL, EPIC), resulting in 7 statistically significant phenotypes, including immune score,

microenvironment score, and macrophage M2, myeloid dendritic cell, CD4+ T cell, and uncharacterized cell (Fig 6 A).

Furthermore, we analyzed the correlation between the risk score, IRGPI genes, the stromal cells, and 28 infiltrating immune cell types through a quantitative scoring system that describes the tumor microenvironment conditions via the Immune Score, Stromal Score, and ESTIMATE score. The Immune Score and Stromal Score are scores based on the degree of enrichment that can be used to evaluate the content of immune cells and stromal cells within the tumor tissue, respectively. The ESTIMATE Score is the sum of them. Together, these scores demonstrate the general phenotype of the tumor microenvironment mathematically. Consequently, the risk score was found negatively related to the Immune Score, and except for S100A1, PSPN, and IL20RB, the other IRGPI genes were significantly related to the aforementioned scores (Fig 6 B). Except for LRSAM1, MET, and PRKCG, the rest were positively associated with the Immune Score, Stromal Score, and ESTIMATE score. The intratumoral heterogeneity was also explored using the Tumor Purity value, with which CXCL11, ERAP2, FYN, GH1, MAP3K14, and SEMA6C were found negatively correlated, while the rest were positively correlated.

In addition, we investigated the relationship between the risk score, IRGPI genes, and diverse infiltrating immune cell types. It was found that the risk score was negatively associated with activated B cells, activated CD8+ T cells, eosinophils, and monocytes, but positively associated with activated CD4+ T cells, CD56dim natural killer cells, central memory CD8+ T cells, Th17 cells, and Th2 cells (Fig 6 C).

The difference in diverse infiltrating immune cell types between the high- and low-risk groups was also investigated. To be more precise, in the high-risk group, the tumor-infiltrating lymphocyte (TIL) is significantly less abundant than that in the low-risk group. Correspondingly, B cells and CD8+ T cells as well as their related activities and partners such as cytolytic activity, T helper cells, etc. are less abundant in the high-risk group than that in the low-risk group, except for MHCI which was almost at the same level between the two groups, and type I IFN receptor which is lower in the high-risk group. The aforementioned findings indicated that the IRGPI-based risk model might serve as a baseline to distinguish different immune cell infiltrating circumstances of individual PAAD patients.

As a supplementary analysis, we also investigated the correlation between the risk score, IRGPI genes, and the well-recognized driver mutation genes including KRAS, TP53, CDKN2A, SMAD4, PIK3CA, MET, STK11, SMARCB1, and JAK3^{[3],[10],[11]}. The results suggested that except for TP53, CDKN2A, and SMARCB1, the expression of all the driver mutation genes was tightly associated with the risk score, and merely the expression of CDKN2A is not associated with all the genes comprising the risk model (Supplementary S4). All in all, to a certain extent, these findings supported the idea that the IRGPI might have deeper implications on the carcinogenesis of PAAD.

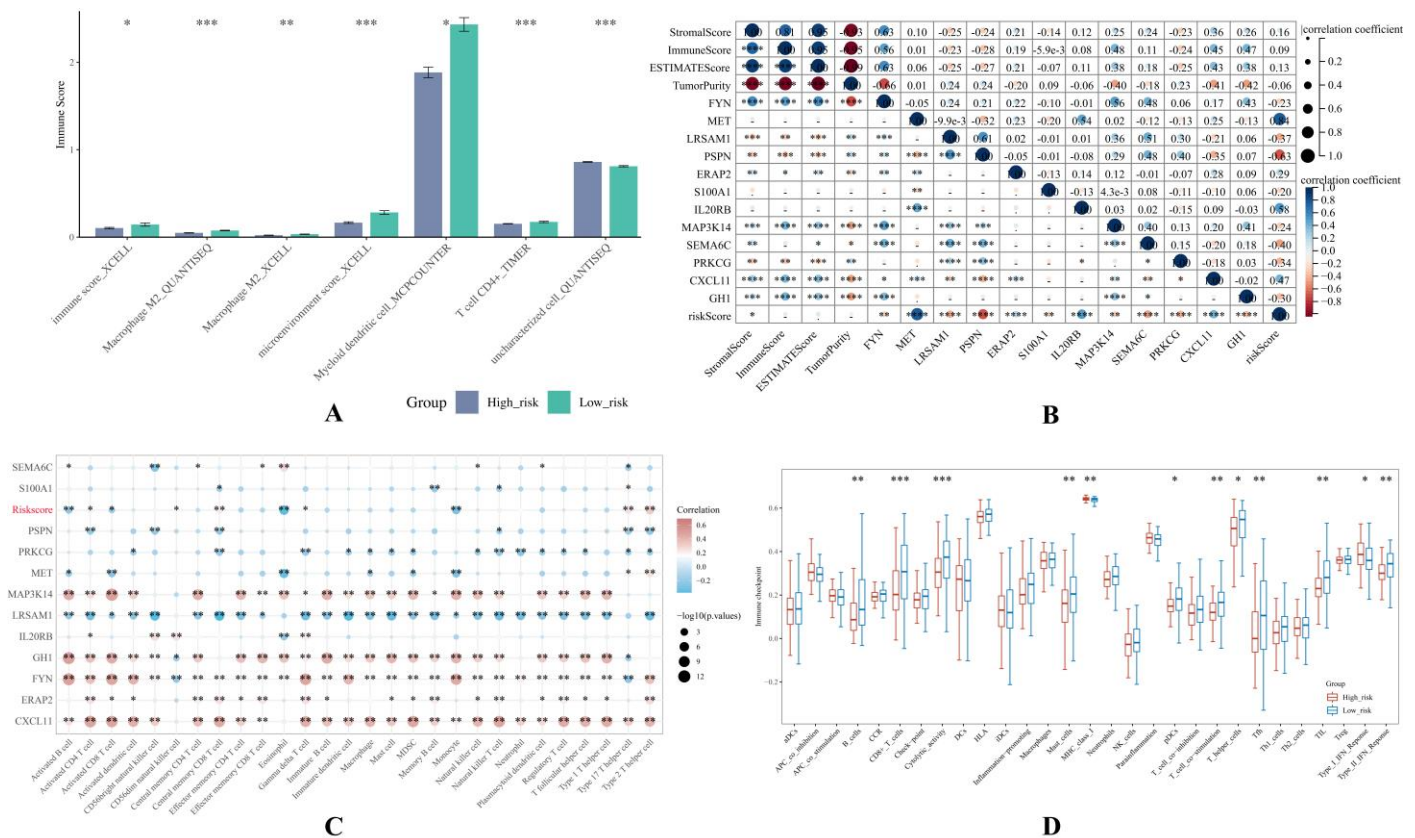


Figure 6. Correlation analysis between the risk score, IRGPI genes, and infiltrating immune cells. (A) The histogram demonstrates the 7 immune-related scores which are statistically different in the high- and low-risk groups. (B) The heatmap demonstrates the correlation between the risk score, IRGPI genes, Immune Score, Stromal Score, ESTIMATE Score, and Tumor Purity value. The black circles represent the definite value of Spearman coefficients, and the color bar represents positivity or negativity. The deeper color in blue means the more negative the Spearman coefficient is. The deeper color in red means the more positive the Spearman coefficient is. (C) The bubble matrix demonstrates the summary of the correlation between the risk score, IRGPI genes, and 28 infiltrating immune cell types. (D) The box plot demonstrates the differences in immune cell infiltration in high- and low-risk groups. In (A)-(D), *, **, and *** represents a P-value < 0.05, P-value < 0.01, and P-value < 0.001, respectively.

PAAD could be more precisely divided into 3 molecular subtypes according to the expression of IRGPI genes

As aforementioned, the high- and low-risk groups possessed distinct OS probability and immunotherapy efficacy, it raised our interest in systemically dividing it into more precise molecular subtypes through the K-means clustering algorithm in an unsupervised manner. It was found that when K-value = 3 (i.e., the TCGA samples were grouped into 3 clusters), the corresponding delta area value reaches its maximum (Fig 7 A). At this point, within the principal component analysis (PCA) diagram, it was observed that the samples were well separated (Fig 7 B). Therefore, ultimately, 3 molecular subtypes were identified and annotated by C1 (N = 157), C2 (N = 13), and C3 (N = 7). We then investigated the clinical outcomes in these molecular subtypes. Results of the survival analysis

suggested that the median survival time of the molecular subtypes is the same which is 1.6 years (Fig 7 C). Furthermore, we examined the expression profiles of the IRGPI genes in each molecular subtype. Consequently, as we expected, except for GH1, they exhibited significant differences in all the subtypes (Fig 7 D).

The result of immune-related score estimation suggested that there were significant differences between the molecular subtypes in the immune score, microenvironment score, and many immune cell types, especially Th1 cell, Th2 cell, CD8⁺ central memory T cell, class-switched memory B cell, and memory B cell (Fig 7 E).

For the analysis of the immune checkpoints, we exhaustively screened all the FDA-approved immune checkpoints up to 2021 including SIGLEC15, TIGIT, CD274, HAVCR2, PDCD1, CTLA4, LAG3, PDCD1LG2, CD276, VTCN1, etc., the result of which showed that in general, subtype 1 demonstrated a more enriched expression profile of these genes, implicating the potential improvement on its immunotherapy. There was also a prominent difference between subtype 2 and subtype 3, implicating that for patients classified into these molecular subtypes, different extents of immunotherapy should be allocated, and different bio-targets should be targeted (Fig 8). Similar to recent *in vitro* and *in vivo* studies reported, the immunotherapy targeting B7 family members, especially B7H3 (i.e., CD276) and B7H4 (i.e., VTCN1), exerted promising efficacy on solid tumors [43]–[47]. Therefore, although the physical barrier in the PAAD tumor microenvironment remains a major obstacle to overcome, our findings may support further optimization of the current immunotherapy strategies.

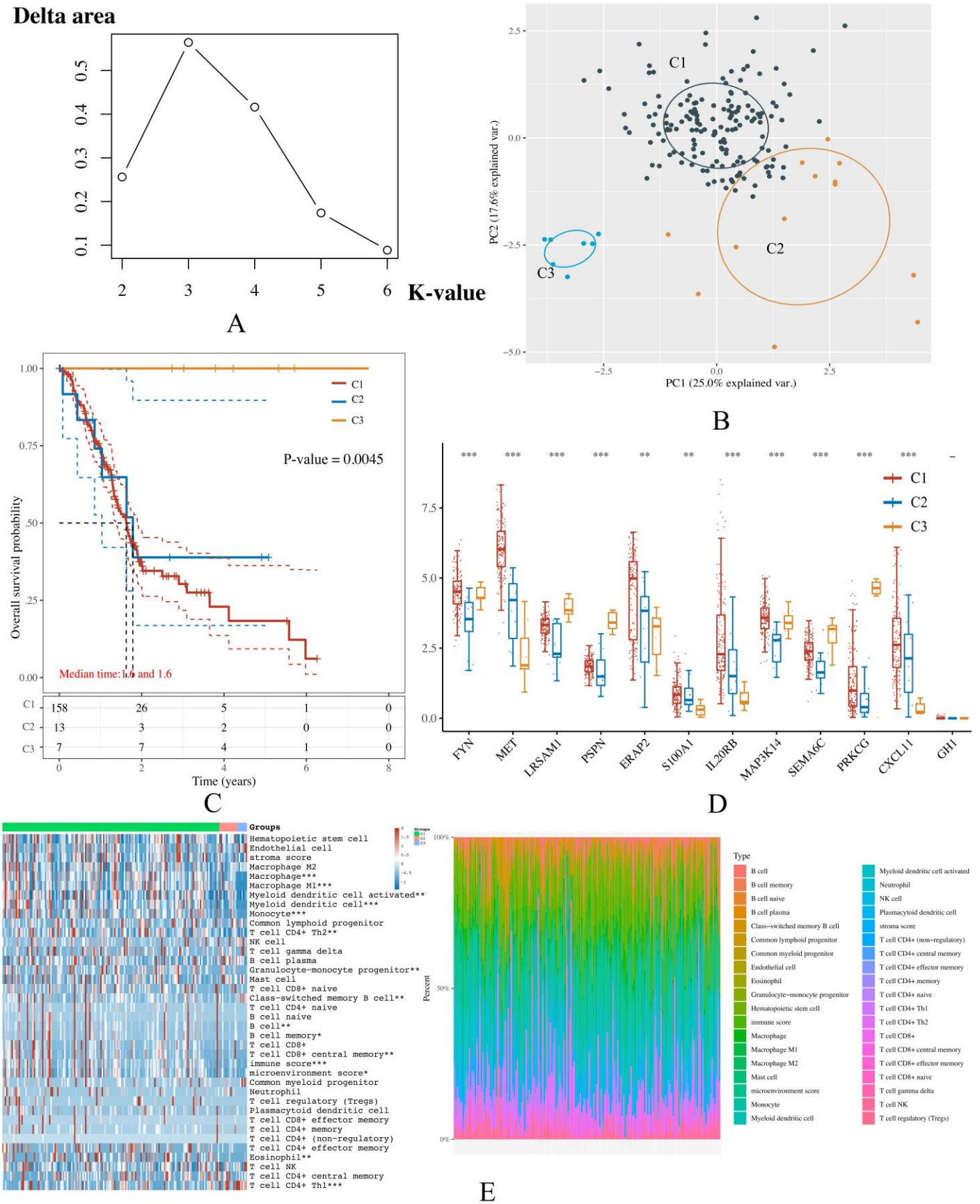


Figure 7. Clustering results for IRGPI-based molecular subtypes. 3 molecular subtypes with optimal consensus values were identified and annotated as C1-3. (A) The delta area diagrams demonstrate the result of clustering through the K-

means algorithm, upon which the most ideal K-value is 3. Therefore, 3 molecular subtypes were deemed most appropriate to be established according to the IRGPI. (B) The principal component analysis (PCA), in which the more widely separated each subtype is, the more ideal the consensus clustering result is achieved. As shown in this panel, 3 subtypes were well separated, once again indicating that clustering the samples in this way is suitable. (C) The Kaplan Meier (KM) curve of the 3 molecular subtypes is annotated as C1-3. (D) The comparison of the IRGPI genes' expression level between each molecular subtype. (E) The heatmap demonstrates different immune-related scores of each molecular subtype on the left and exhibits the abundance of each immune cell type on the right. The x-axis represents the TCGA samples involved in the analysis. In (D)-(E), *, **, and *** represents a P-value < 0.05, P-value < 0.01, and P-value < 0.001, respectively.

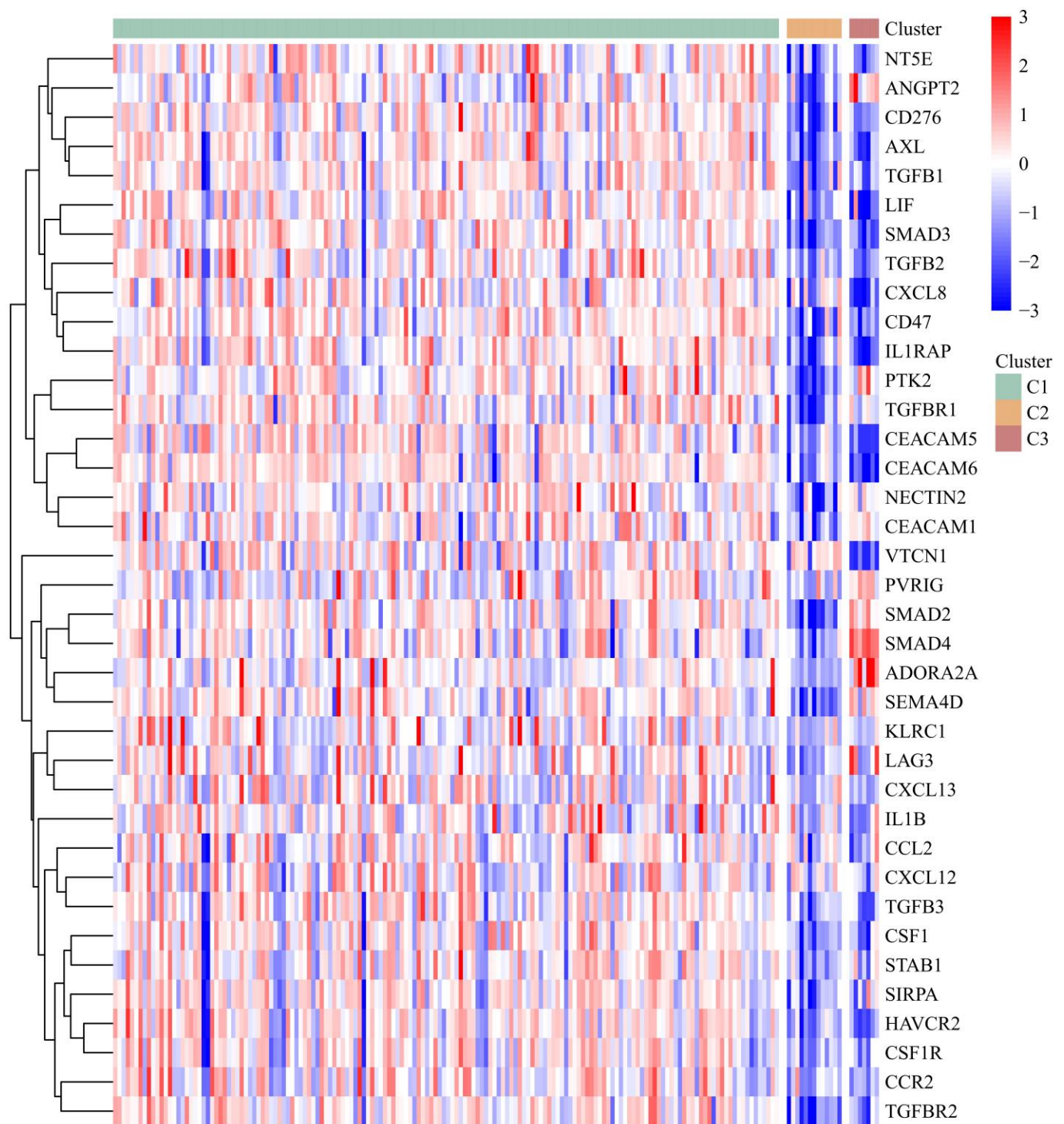


Figure 8. The heatmap displays the expression of the representative genes of the currently FDA-approved immune checkpoints in different IRGPI-based molecular subtypes. The x-axis represents the TCGA samples involved in the analysis. The red color indicates a positive correlation, while the blue color indicates the opposite.

Discussion

The long-term survival rates of most cancer types have vastly improved as a result of the evolution of modern medical technology. However, pancreatic adenocarcinoma (PAAD) remains the most fatal malignancy ^{[1],[2]}. As such, evaluation of clinical outcomes is essential in both financial and humanitarian dimensions. Therefore, we developed a novel immune-related gene prognostic index (IRGPI) consisting of 12 genes including FYN, MET, LRSAM1, PSPN, ERAP2, S100A1, IL20RB, MAP3K14, SEMA6C, PRKCG, CXCL11, GH1 with a corresponding risk model for OS prediction. In conjunction with other clinical factors, a nomogram was further constructed. Additionally, the risk model was evaluated using external datasets and compared to existing ones, suggesting that our model's performance was more robust and accurate.

According to the previous study, FYN, LRSAM1, and SEMA6C serve as poor prognostic biomarkers in pancreatic cancer, whereas ERAP2, MET, IL20RB, and CXCL11 indicate improvements. Interestingly, FYN, LRSAM1, IL20RB, CXCL11, S100A1, and MAP3K14 are also well-recognized biomarkers in the prognosis of renal cancer, which is reminiscent of the pancreatic metastasis from renal cell carcinoma in some earlier studies ^{[48]-[50]}. **Of note that recent advances in kinome study revealed that multiple emerging kinase targets might play as rising stars in the treatment of digestive cancers ^{[51]-[53]}. Among them, the FYN proto-oncogene kinase was lately proven to have increased activity in specific cancer types, including pancreatic cancer. FYN-related kinase has been especially highlighted as it not only directly contributes to pancreatic cell proliferation and migration, but also contributes to the development, progression, and maintenance of the inflammatory stroma by promoting desmoplasia, which is in part responsible for resistance to treatment in pancreatic cancer ^{[54],[55]}.**

As for GH1, PRKCG, and PSPN, they are not known prognostic biomarkers, but GH1 is still regarded as strongly related to cancer development because of its key role in the stimulation of growth factor secretion (i.e., IGF-1) ^[56]. PRKCG and PSPN have a function in neurodegenerative diseases ^[48]. In the present study, additional enrichment analyses revealed that these IRGPI genes are primarily associated with immunological processes and abnormal cell proliferation.

Furthermore, we investigated IRGPI as a risk model in the tumor microenvironment and at the single-gene level. The tumor microenvironment as one of the most critical obstacles in PAAD has been studied extensively. In a literature review, Sofia Liot et. al. summarized the cellular characteristics as exhaustion of anti-cancer cytotoxic T lymphocytes and the infiltration of multiple types of tumor-promoting immune cells ^[57]. In animal experiments, Clark CE et. al. reported that tumor-associated macrophages, myeloid-derived suppressor cells, and regulatory T cells (Tregs) appear in the early precursor lesions of PC and persist through invasive cancer in the mouse ^[58]. **Interestingly the transcription factors characteristic of Tregs (i.e., FOXP3 and ROR γ t) were not identified as prognostic factors in the current evaluation, despite their reported persistence in invasive cancer. This might be due to the dual role of these cells in these types of tumors ^[59], where they have exhibited both pro- and anti-inflammatory effects.** In clinical practice, Fukunaga et. al. observed that CD8+ tumor-infiltrating lymphocytes together with CD4+ tumor-infiltrating lymphocytes and dendritic cells are found associated with improved postoperative survival ^[60], whereas the same was not present when CD8+ and CD4+ cells were present alone without the other population. The tumor-

associated macrophages found in pancreatic cancer models can also prevent T cells from infiltrating the tumor leading to T cell exclusion in some tumors [40]-[42],[61]. Cancer-associated fibroblasts contribute to this effect by molding the extracellular environment to limit T cell infiltration, and by secreting cytokines that can limit effector cell functions [62]-[65].

The role of other immune cells should not be discounted, either. Dendritic cells have been identified as an independent prognostic factor for PAAD [66], with lower circulating dendritic cell numbers resulting in a worse prognosis [67]. Tumor-associated macrophages also interface with tumor-associated neutrophils, with the overall effect of driving tumor progression through the promotion of hypoxia, vascular remodeling, fibrosis, immunosuppression, and metastasis formation [68]. In short, despite some less-satisfying attempts, randomized clinical trials targeting the tumor microenvironment are still ongoing, and research on crosstalks between the risk score, IRGPI genes, stromal cells, and immune cells is in demand. Therefore, in the present study, starting from evaluating the general appearance of the tumor microenvironment, we qualitatively analyzed the content of stromal cells and 28 infiltrating immune cell types in high- and low-risk groups. We found that these groups were quite distinct from one another, indicating that the IRGPI was potentially connected to the tumor microenvironment. The results of the correlation analysis between the risk score and the tumor microenvironment once again supported such ideas.

Based on the IRGPI genes, we clustered PAAD into 3 distinct molecular subtypes in a more precise way, demonstrating distinct correlations with the expression of currently FDA-approved immune checkpoints, providing a new insight for future precision and translational medicine.

Supplementary materials: S1_List of the 149 DEIRGs that were significantly related to the OS of PAAD patients. S2_Process of feature gene selection. S3_Expression analysis of IRGPI genes. S4_Correlation between the risk score, IRGPI genes, and driver mutation genes.

Author Contributions: Conceptualization, Shujing Zhou; methodology, Shujing Zhou; software, Xufeng Huang; validation, Xufeng Huang; formal analysis, Shujing Zhou; investigation, Shujing Zhou; resources, Shujing Zhou; data curation, Shujing Zhou; writing—original draft preparation, Xufeng Huang; writing—review and editing, Attila Gábor Szöllósi, Yi Che Chang Chien, and András Hajdu; visualization, Xufeng Huang, Attila Gábor Szöllósi, and András Hajdu; supervision, Yi Che Chang Chien and András Hajdu; project administration, Xufeng Huang; funding acquisition, András Hajdu. All authors have read and agreed to the published version of the manuscript.

Funding: This work is funded in part by the project TKP2021-NKTA-34, implemented with the support provided by the National Research, Development, and Innovation Fund of Hungary under the TKP2021-NKTA funding scheme.

Institutional Review Board Statement: Not applicable.

Informed Consent Statement: Not applicable.

Data Availability Statement: The datasets presented in this study can be found in online repositories. The names of the repository/repositories and accession number(s) can be found in the article or supplementary materials.

Acknowledgments: We sincerely thank the **National Research, Development and Innovation Fund of Hungary**, the Tempus public foundation, and the Chinese scholarship council for their financial support to the author, which made it possible to cover the article processing fee of the present study.

Conflicts of Interest: The authors declare that the research was conducted in the absence of any commercial or financial relationships that could be construed as a potential conflict of interest.

References

- [1] Karamitopoulou, E. Molecular Pathology of Pancreatic Cancer. *Cancers* 2022, 14, 1523. <https://doi.org/10.3390/cancers14061523>
- [2] Nevala-Plagemann C, Hidalgo M, Garrido-Laguna I. From state-of-the-art treatments to novel therapies for advanced-stage pancreatic cancer. *Nat Rev Clin Oncol.* 2020 Feb;17(2):108-123. doi: 10.1038/s41571-019-0281-6. Epub 2019 Nov 8. PMID: 31705130.
- [3] Nollmann FI, Ruess DA. Targeting Mutant KRAS in Pancreatic Cancer: Futile or Promising? *Biomedicines.* 2020 Aug 11;8(8):281. doi: 10.3390/biomedicines8080281. PMID: 32796566; PMCID: PMC7459579.
- [4] Chandan S, Deliwala SS, Facciorusso A, Mohan BP, Ramai D, Kochhar GS. Association of BRCA Mutations and Pancreatic Cancer: Review of Literature and Meta-analysis. *Pancreas.* 2022 Jan 1;51(1):e8-e10. doi: 10.1097/MPA.0000000000001956. PMID: 35195609.
- [5] Cellini F, Arcelli A, Simoni N, Caravatta L, Buwenge M, Calabrese A, Brunetti O, Genovesi D, Mazzarotto R, Deodato F, Mattiucci GC, Silvestris N, Valentini V, Morganti AG. Basics and Frontiers on Pancreatic Cancer for Radiation Oncology: Target Delineation, SBRT, SIB technique, MRgRT, Particle Therapy, Immunotherapy and Clinical Guidelines. *Cancers (Basel).* 2020 Jun 29;12(7):1729. doi: 10.3390/cancers12071729. PMID: 32610592; PMCID: PMC7407382.
- [6] Ambe C, Fulp W, Springett G, Hoffe S, Mahipal A. A Meta-analysis of Randomized Clinical Trials of Chemoradiation Therapy in Locally Advanced Pancreatic Cancer. *J Gastrointest Cancer.* 2015 Sep;46(3):284-90. doi: 10.1007/s12029-015-9734-z. PMID: 26018826.
- [7] Martín AM, Hidalgo M, Alvarez R, Arrazubi V, Martínez-Galán J, Salgado M, Macarulla T, Carrato A. From First Line to Sequential Treatment in the Management of Metastatic Pancreatic Cancer. *J Cancer.* 2018 Apr 30;9(11):1978-1988. doi: 10.7150/jca.23716. PMID: 29896283; PMCID: PMC5995948.
- [8] Ambe C, Fulp W, Springett G, Hoffe S, Mahipal A. A Meta-analysis of Randomized Clinical Trials of Chemoradiation Therapy in Locally Advanced Pancreatic Cancer. *J Gastrointest Cancer.* 2015 Sep;46(3):284-90. doi: 10.1007/s12029-015-9734-z. PMID: 26018826.
- [9] Perales-Patón J, Piñeiro-Yañez E, Tejero H, López-Casas PP, Hidalgo M, Gómez-López G, Al-Shahrour F. Pancreas Cancer Precision Treatment Using Avatar Mice from a Bioinformatics Perspective. *Public Health Genomics.* 2017;20(2):81-91. doi: 10.1159/000479812. Epub 2017 Sep 1. PMID: 28858862.

- [10] Singh, K. et al. Kras mutation rate precisely orchestrates ductal derived pancreatic intraepithelial neoplasia and pancreatic cancer. *Lab. Invest.* 101, 177–192 (2021).
- [11] Buscail, L., Bournet, B. & Cordelier, P. Role of oncogenic KRAS in the diagnosis, prognosis and treatment of pancreatic cancer. *Nat. Rev. Gastroenterol. Hepatol.* 17, 153–168 (2020).
- [12] Qian, Y. et al. Molecular alterations and targeted therapy in pancreatic ductal adenocarcinoma. *J. Hematol. Oncol.* 13, 130 (2020).
- [13] Mizrahi, J. D., Surana, R., Valle, J. W. & Shroff, R. T. Pancreatic cancer. *Lancet* 395, 2008–2020 (2020).
- [14] Christenson, E. S., Jaffee, E. & Azad, N. S. Current and emerging therapies for patients with advanced pancreatic ductal adenocarcinoma: a bright future. *Lancet Oncol.* 21, e135–e145 (2020).
- [15] Dardare, J., Witz, A., Merlin, J. L., Gilson, P. & Harlé, A. SMAD4 and the TGF β pathway in patients with pancreatic ductal adenocarcinoma. *Int. J. Mol. Sci.* 21, 3534 (2020).
- [16] Connor, A. A. et al. Integration of genomic and transcriptional features in pancreatic cancer reveals increased cell cycle progression in metastases. *Cancer Cell* 35, 267–282.e267 (2019).
- [17] Yang J, Wei X, Hu F, Dong W, Sun L. Development and validation of a novel 3-gene prognostic model for pancreatic adenocarcinoma based on ferroptosis-related genes. *Cancer Cell Int.* 2022 Jan 15;22(1):21. doi: 10.1186/s12935-021-02431-8. PMID: 35033072; PMCID: PMC8760727.
- [18] Bai Z, Xu F, Feng X, Wu Y, Lv J, Shi Y, Pei H. Pyroptosis regulators exert crucial functions in prognosis, progression and immune microenvironment of pancreatic adenocarcinoma: a bioinformatic and in vitro research. *Bioengineered.* 2022 Jan;13(1):1717-1735. doi: 10.1080/21655979.2021.2019873. PMID: 35000541; PMCID: PMC8805829.
- [19] Yang, F., Bettadapura, S.N., Smeltzer, M.S. et al. Pyroptosis and pyroptosis-inducing cancer drugs. *Acta Pharmacol Sin* (2022). <https://doi.org/10.1038/s41401-022-00887-6>
- [20] Hiam-Galvez, K.J., Allen, B.M. & Spitzer, M.H. Systemic immunity in cancer. *Nat Rev Cancer* 21, 345–359 (2021). <https://doi.org/10.1038/s41568-021-00347-z>
- [21] Binnewies, M., Roberts, E.W., Kersten, K. et al. Understanding the tumor immune microenvironment (TIME) for effective therapy. *Nat Med* 24, 541–550 (2018). <https://doi.org/10.1038/s41591-018-0014-x>
- [22] Cancer Genome Atlas Research Network, Weinstein JN, Collisson EA, et al. The Cancer Genome Atlas Pan-Cancer analysis project. *Nat Genet.* 2013;45(10):1113-1120. doi:10.1038/ng.2764
- [23] International Cancer Genome Consortium, Hudson TJ, Anderson W, et al. International network of cancer genome projects [published correction appears in *Nature*. 2010 Jun 17;465(7300):966. Himmelbaue, Heinz [corrected to Himmelbauer, Heinz];

- Gardiner, Brooke A [corrected to Gardiner, Brooke B]; Cross, Anthony [corrected to Cross, Anthony]]. *Nature*. 2010;464(7291):993-998. doi:10.1038/nature08987
- [24] Lonsdale, J., Thomas, J., Salvatore, M. et al. The Genotype-Tissue Expression (GTEx) project. *Nat Genet* 45, 580–585 (2013). <https://doi.org/10.1038/ng.2653>
- [25] Bhattacharya S, Dunn P, Thomas CG, et al. ImmPort, toward repurposing of open access immunological assay data for translational and clinical research. *Sci Data*. 2018; 5:180015. Published 2018 Feb 27. doi:10.1038/sdata.2018.15
- [26] Ji Z, Vokes S, Dang C, Ji H (2015). “Turning publicly available gene expression data into discoveries using gene set context analysis.” *Nucleic Acids Res.* gkv873.
- [27] Ritchie ME, Phipson B, Wu D, et al. limma powers differential expression analyses for RNA-sequencing and microarray studies. *Nucleic Acids Res.* 2015;43(7): e47. doi:10.1093/nar/gkv007
- [28] Wickham H (2016). ggplot2: Elegant Graphics for Data Analysis. Springer-Verlag New York. ISBN 978-3-319-24277-4, <https://ggplot2.tidyverse.org>.
- [29] Philippe Bardou, Jérôme Mariette, Frédéric Escudié, Christophe Djemiel and Christophe Klopp. jvenn: an interactive Venn diagram viewer. *BMC Bioinformatics* 2014, 15:293 doi:10.1186/1471-2105-15-293
- [30] Friedman J, Hastie T, Tibshirani R. Regularization Paths for Generalized Linear Models via Coordinate Descent. *J Stat Softw.* 2010;33(1):1-22. PMID: 20808728; PMCID: PMC2929880.
- [31] Blanche P, Dartigues J, Jacqmin-Gadda H (2013). “Estimating and Comparing time-dependent areas under receiver operating characteristic curves for censored event times with competing risks.” *Statistics in Medicine*, 32(30), 5381–5397. <http://onlinelibrary.wiley.com/doi/10.1002/sim.5958/full>.
- [32] Terry M. Therneau, Patricia M. Grambsch (2000). *Modeling Survival Data: Extending the Cox Model*. Springer, New York. ISBN 0-387-98784-3.
- [33] Taiwen Li, Jingxin Fu, Zexian Zeng, David Cohen, Jing Li, Qianming Chen, Bo Li, X Shirley Liu, TIMER2.0 for analysis of tumor-infiltrating immune cells, *Nucleic Acids Research*, Volume 48, Issue W1, 02 July 2020, Pages W509–W514, <https://doi.org/10.1093/nar/gkaa407>
- [34] Sturm G, Finotello F, List M. Immunedeconv: An R Package for Unified Access to Computational Methods for Estimating Immune Cell Fractions from Bulk RNA-Sequencing Data. *Methods in Molecular Biology (Clifton, N.J.)*. 2020 ;2120:223-232. DOI: 10.1007/978-1-0716-0327-7_16. PMID: 32124323.
- [35] Newman AM, Liu CL, Green MR, et al. Robust enumeration of cell subsets from tissue expression profiles. *Nat Methods*. 2015;12(5):453-457. doi:10.1038/nmeth.3337
- [36] Ya-Ru Miao, Mengxuan Xia, Mei Luo, Tao Luo, Mei Yang, An-Yuan Guo, ImmuCellAI-mouse: a tool for comprehensive prediction of mouse immune cell abundance and immune microenvironment depiction, *Bioinformatics*, 2021;; btab711. <https://doi.org/10.1093/bioinformatics/btab711>
- [37] Wilkerson, D. M, Hayes, Neil D (2010). “ConsensusClusterPlus: a class discovery tool with confidence assessments and item tracking.” *Bioinformatics*, 26(12), 1572-1573. <http://bioinformatics.oxfordjournals.org/content/26/12/1572.abstract>.
- [38] Sun, W., Jiang, Y. Z., Liu, Y. R., Ma, D., & Shao, Z. M. (2016). Nomograms to estimate long-term overall survival and breast cancer-specific survival of patients with luminal breast cancer. *Oncotarget*, 7(15), 20496–20506. <https://doi.org/10.18632/oncotarget.7975>

- [39] Hu, J. Q., Yu, P. C., Shi, X., Liu, W. L., Zhang, T. T., Lei, B. W., Huang, N. S., Xu, W. B., Han, L. T., Ma, B., Liao, T., Wei, W. J., Wang, Y., Lu, Z. W., Wang, Y. L., & Ji, Q. H. (2019). Prognostic Nomograms for Predicting Overall Survival and Cancer-Specific Survival of Patients with Major Salivary Gland Mucoepidermoid Carcinoma. *Journal of Cancer*, 10(18), 4380–4388. <https://doi.org/10.7150/jca.27992>
- [40] Joyce, Johanna A, and Douglas T Fearon. "T cell exclusion, immune privilege, and the tumor microenvironment." *Science (New York, N.Y.)* vol. 348,6230 (2015): 74-80. doi:10.1126/science.aaa6204
- [41] Anderson, Kristin G et al. "Obstacles Posed by the Tumor Microenvironment to T cell Activity: A Case for Synergistic Therapies." *Cancer cell* vol. 31,3 (2017): 311-325. doi: 10.1016/j.ccell.2017.02.008
- [42] Hosein AN, Brekken RA, Maitra A. Pancreatic cancer stroma: an update on therapeutic targeting strategies. *Nat Rev Gastroenterol Hepatol.* (2020) 17:487–505. doi: 10.1038/s41575-020-0300-1
- [43] Lee, Yh., Martin-Orozco, N., Zheng, P. et al. Inhibition of the B7-H3 immune checkpoint limits tumor growth by enhancing cytotoxic lymphocyte function. *Cell Res* 27, 1034–1045 (2017). <https://doi.org/10.1038/cr.2017.90>
- [44] Picarda E, Ohaegbulam KC, Zang X. Molecular Pathways: Targeting B7-H3 (CD276) for Human Cancer Immunotherapy. *Clin Cancer Res.* 2016 Jul 15;22(14):3425-3431. doi: 10.1158/1078-0432.CCR-15-2428. Epub 2016 May 20. PMID: 27208063; PMCID: PMC4947428.
- [45] Dong P, Xiong Y, Yue J, Hanley SJB, Watari H. B7H3 As a Promoter of Metastasis and Promising Therapeutic Target. *Front Oncol.* 2018; 8:264. Published 2018 Jul 6. doi:10.3389/fonc.2018.00264
- [46] Podojil JR, Miller SD. Potential targeting of B7-H4 for the treatment of cancer. *Immunol Rev.* 2017;276(1):40-51. doi:10.1111/imr.12530
- [47] Heather L. MacGregor, Pamela S. Ohashi; Molecular Pathways: Evaluating the Potential for B7-H4 as an Immunoregulatory Target. *Clin Cancer Res* 15 June 2017; 23 (12): 2934–2941. <https://doi.org/10.1158/1078-0432.CCR-15-2440>
- [48] Uhlén M, Fagerberg L, Hallström BM, Lindskog C, Oksvold P, Mardinoglu A, Sivertsson Å, Kampf C, Sjöstedt E, Asplund A, Olsson I, Edlund K, Lundberg E, Navani S, Szigartyo CA, Odeberg J, Djureinovic D, Takanen JO, Hober S, Alm T, Edqvist PH, Berling H, Tegel H, Mulder J, Rockberg J, Nilsson P, Schwenk JM, Hamsten M, von Feilitzen K, Forsberg M, Persson L, Johansson F, Zwahlen M, von Heijne G, Nielsen J, Pontén F. Tissue-based map of the human proteome. *Science* 2015 347(6220):1260419. PubMed: 25613900 DOI: 10.1126/science.1260419
- [49] Abdul-Ghafar, J., Ud Din, N., Saadaat, R. et al. Metastatic renal cell carcinoma to pancreas and gastrointestinal tract: a clinicopathological study of 3 cases and review of literature. *BMC Urol* 21, 84 (2021). <https://doi.org/10.1186/s12894-021-00854-z>
- [50] Ballarin R, Spaggiari M, Cautero N, et al. Pancreatic metastases from renal cell carcinoma: the state of the art. *World J Gastroenterol.* 2011;17(43):4747-4756. doi:10.3748/wjg.v17.i43.4747
- [51] Bhullar, K.S., Lagarón, N.O., McGowan, E.M. et al. Kinase-targeted cancer therapies: progress, challenges and future directions. *Mol Cancer* 17, 48 (2018). <https://doi.org/10.1186/s12943-018-0804-2>
- [52] Morishita, A., Gong, J., & Masaki, T. (2014). Targeting receptor tyrosine kinases in gastric cancer. *World journal of gastroenterology*, 20(16), 4536–4545. <https://doi.org/10.3748/wjg.v20.i16.4536>

- [53] Creeden, J. F., Kipp, Z. A., Xu, M., Flight, R. M., Moseley, H., Martinez, G. J., Lee, W. H., Alganem, K., Imami, A. S., McMullen, M. R., Roychowdhury, S., Nawabi, A. M., Hipp, J. A., Softic, S., Weinman, S. A., McCullumsmith, R., Nagy, L. E., & Hinds, T. D., Jr (2022). Hepatic kinome atlas: An in-depth identification of kinase pathways in liver fibrosis of humans and rodents. *Hepatology* (Baltimore, Md.), 10.1002/hep.32467. Advance online publication. <https://doi.org/10.1002/hep.32467>
- [54] Creeden, J.F.; Alganem, K.; Imami, A.S.; Henkel, N.D.; Brunicardi, F.C.; Liu, S.-H.; Shukla, R.; Tomar, T.; Naji, F.; McCullumsmith, R.E. Emerging Kinase Therapeutic Targets in Pancreatic Ductal Adenocarcinoma and Pancreatic Cancer Desmoplasia. *Int. J. Mol. Sci.* 2020, 21, 8823. <https://doi.org/10.3390/ijms21228823>
- [55] Creeden, J.F.; Alganem, K.; Imami, A.S.; Brunicardi, F.C.; Liu, S.-H.; Shukla, R.; Tomar, T.; Naji, F.; McCullumsmith, R.E. Kinome Array Profiling of Patient-Derived Pancreatic Ductal Adenocarcinoma Identifies Differentially Active Protein Tyrosine Kinases. *Int. J. Mol. Sci.* 2020, 21, 8679. <https://doi.org/10.3390/ijms21228679>
- [56] Thadani A, Pais S, Savino J. Metastasis of renal cell carcinoma to the pancreas 13 years postnephrectomy. *Gastroenterol Hepatol* (N Y). 2011;7(10):697-699.
- [57] Liot, Sophie et al. "Stroma Involvement in Pancreatic Ductal Adenocarcinoma: An Overview Focusing on Extracellular Matrix Proteins." *Frontiers in immunology* vol. 12 612271. 6 Apr. 2021, doi:10.3389/fimmu.2021.612271
- [58] Clark CE, Hingorani SR, Mick R, et al. Dynamics of the immune reaction to pancreatic cancer from inception to invasion. *Cancer Res* 2007; 67:9518–27.
- [59] Chellappa, Stalin et al. "Regulatory T cells that co-express ROR γ t and FOXP3 are pro-inflammatory and immunosuppressive and expand in human pancreatic cancer." *Oncoimmunology* vol. 5,4 e1102828. 29 Oct. 2015, doi:10.1080/2162402X.2015.1102828
- [60] Fukunaga A, Miyamoto M, Cho Y, et al. CD8+ tumor-infiltrating lymphocytes together with CD4+ tumor-infiltrating lymphocytes and dendritic cells improve the prognosis of patients with pancreatic adenocarcinoma. *Pancreas*. 2004;28: e26–31.
- [61] Zhu, Yu et al. "CSF1/CSF1R blockade reprograms tumor-infiltrating macrophages and improves response to T-cell checkpoint immunotherapy in pancreatic cancer models." *Cancer research* vol. 74,18 (2014): 5057-69. doi: 10.1158/0008-5472.CAN-13-3723
- [62] Vonderheide, Robert H, and Adham S Bear. "Tumor-Derived Myeloid Cell Chemoattractants and T Cell Exclusion in Pancreatic Cancer." *Frontiers in immunology* vol. 11 605619. 10 Nov. 2020, doi:10.3389/fimmu.2020.605619
- [63] Sahai, Erik et al. "A framework for advancing our understanding of cancer-associated fibroblasts." *Nature reviews. Cancer* vol. 20,3 (2020): 174-186. doi:10.1038/s41568-019-0238-1
- [64] Öhlund, Daniel et al. "Distinct populations of inflammatory fibroblasts and myofibroblasts in pancreatic cancer." *The Journal of experimental medicine* vol. 214,3 (2017): 579-596. doi:10.1084/jem.20162024
- [65] Feig, Christine et al. "Targeting CXCL12 from FAP-expressing carcinoma-associated fibroblasts synergizes with anti-PD-L1 immunotherapy in pancreatic cancer." *Proceedings of the National Academy of Sciences of the United States of America* vol. 110,50 (2013): 20212-7. doi:10.1073/pnas.1320318110
- [66] Hirooka, Satoshi et al. "The role of circulating dendritic cells in patients with unresectable pancreatic cancer." *Anticancer research* vol. 31,11 (2011): 3827-34.

[67] Yanagimoto, Hiroaki et al. "Impaired function of circulating dendritic cells in patients with pancreatic cancer." *Clinical immunology (Orlando, Fla.)* vol. 114,1 (2005): 52-60. doi:10.1016/j.clim.2004.09.007

[68] Pratt, Hillary G et al. "Macrophage and Neutrophil Interactions in the Pancreatic Tumor Microenvironment Drive the Pathogenesis of Pancreatic Cancer." *Cancers* vol. 14,1 194. 31 Dec. 2021, doi:10.3390/cancers14010194